



Experimental investigation of the effect of inclination angle on convection-driven melting of phase change material in a rectangular enclosure



Babak Kamkari ^{a,*}, Hossein Shokouhmand ^a, Frank Bruno ^b

^a School of Mechanical Engineering, College of Engineering, University of Tehran, Tehran 14395-515, Iran

^b Barbara Hardy Institute, University of South Australia, Mawson Lakes, SA 5095, Australia

ARTICLE INFO

Article history:

Received 17 September 2013

Received in revised form 23 December 2013

Accepted 3 January 2014

Keywords:

Phase change material

Natural convection

Heat transfer enhancement

Thermal storage

Inclination angle

Melting

ABSTRACT

This paper investigates the dynamic thermal behavior of phase change material (PCM) melting in a rectangular enclosure at various inclination angles. Lauric acid as a PCM with high Prandtl number ($Pr \approx 100$) is used. The enclosure is heated isothermally from one side while the other walls are thermally insulated. Experiments were performed with hot wall temperatures of 55, 60 and 70 °C ($3.6 \times 10^8 \leq Ra \leq 8.3 \times 10^8$) for different inclination angles of 0°, 45° and 90°. Image processing of melt photographs along with recorded temperatures were used to calculate the melt fractions, Nusselt numbers and the local interfacial heat transfer rates at the solid–liquid interface. Qualitative time-dependent natural convection flow structures were deduced indirectly from the instantaneous shape of the solid–liquid interface which were confirmed by quantitative data from temperature measurements. The results reveal that the enclosure inclination has a significant effect on the formation of natural convection currents and consequently on the heat transfer rate and melting time of the PCM. As the inclination angle is decreased from 90° to 0°, the convection currents in the enclosure increases and chaotic flow structures appear. When melting commences in the horizontally inclined enclosure, the solid–liquid interface line becomes wavy which implies the formation of Benard convection cells in the liquid PCM. For the same hot wall temperatures, a decrease in inclination angle leads to a considerable enhancement in energy transport from the hot wall of the enclosure to the PCM. It is found that the heat transfer enhancement ratio for the horizontal enclosure is more than two times higher than that of the vertical enclosure.

© 2014 Elsevier Ltd. All rights reserved.

1. Introduction

Solid–liquid phase change problems in relation to phase change materials (PCMs) have been of growing interest in recent decades. PCMs are attractive as they are capable of absorbing and releasing a considerable amount of energy at a nearly constant temperature during the melting and solidification processes. They can be incorporated into various thermal systems where their latent heat is utilized for thermal storage purposes or heat rejection. There is a wide range of applications for PCMs such as solar thermal systems [1,2], desalination [3], heat recovery [4], buildings [5,6], refrigeration [7], thermal management of electronics [8,9], space crafts [10,11], and smart textile [12]. In order to maximize the thermal performance of systems using PCMs, a better understanding of the thermal behavior of the PCM is required. Over the past decades, several investigations have been performed to study the role of natural

convection on the melting heat transfer and morphology of the solid–liquid interface. These studies are classified into two groups based on the Prandtl number of the PCM employed in the investigation; low Prandtl number ($Pr < 1$) and high Prandtl number ($Pr \geq 1$) PCMs.

Metallic PCMs have a high thermal conductivity and are categorized as low Prandtl number PCMs. One of the first studies in this field was conducted by Gau and Viskanta [13]. The role of the natural convection on the solid–liquid interface motion of pure gallium ($Pr \approx 0.021$) was studied during melting from below and solidification from above in a rectangular enclosure. Different natural convection flow regimes were identified and it was found that the turbulent natural convection within the liquid PCM considerably distorts the solid–liquid interface and increases the melting rate. They also reported similar findings when they commenced melting a lipowitz eutectic from the bottom in a rectangular cavity ($Pr \approx 0.067$) [14]. In another experimental work by the same investigators [15], the influence of natural convection on the melting heat transfer during phase change of gallium on a vertical wall was studied. Despite the high thermal conductivity of metallic

* Corresponding author. Tel.: +98 9124034778; fax: +98 2188013029.

E-mail addresses: kamkari@ut.ac.ir (B. Kamkari), hshokoh@ut.ac.ir (H. Shokouhmand), frank.bruno@unisa.edu.au (F. Bruno).

Nomenclature

A_w	area of heated wall (m^2)	$Ra = \frac{g\beta(T_w - T_m)H^3}{\nu\eta}$	Rayleigh number on hot wall of the enclosure
H	height of the rectangular enclosure (m)	t	time (t)
\bar{h}	average heat transfer coefficient ($\text{W}/\text{m}^2 \text{K}$)	T	temperature ($^\circ\text{C}$)
k	thermal conductivity ($\text{W}/\text{m K}$)	T_m	melting temperature ($^\circ\text{C}$)
$\overline{Nu}(t)$	surface-average Nusselt number	T_w	hot wall temperature ($^\circ\text{C}$)
$\langle \overline{Nu} \rangle$	time-average Nusselt number		
Pr	Prandtl number		
Q_{loss}	heat loss from the enclosure (kJ)		

PCM which can increase the role of conduction heat transfer, it was established that the solid–liquid interface shape and the melting rate are greatly affected by the laminar buoyancy driven natural convection. The evaluation of the effect of the convection currents on melting of tin ($Pr \approx 0.009$) in a rectangular enclosure was considered by Wolf and Viskanta [16]. The results revealed that the shape of the solid–liquid interface is not greatly affected by natural convection in the liquid metal. This was attributed to the high thermal conductivity of tin ($k \approx 60 \text{ W}/\text{m K}$) in comparison with non-metallic PCMs which makes the conduction heat transfer as the dominant mode of heat transfer. Beckermann and Viskanta [17] examined the influence of subcooling of the solid phase of gallium on buoyancy driven melting in a rectangular enclosure. It was found that solid subcooling significantly reduces the melting rate when compared to melting of the solid at the melting temperature.

Despite the high thermal conductivity of metallic PCMs which augments the heat transfer rate, they are rarely used for real applications due to their high cost, low or very high melting temperature and high density.

Examples of the second group of PCMs which possess high Prandtl numbers are Water, paraffins and fatty acids. One of the first studies in this field was performed by Boger and Westwater [18]. They investigated the effect of buoyancy on melting and freezing of water ($Pr \approx 10$). Their results on the effect of buoyancy and density change on the melting rate of water cannot be generalized due to the density inversion of water which is unique to this substance. The significant influence of natural convection currents on the shape of the solid–liquid interface and heat transfer rate when melting *n*-octadecane ($Pr \approx 68$) from the bottom has been reported by Hale and Viskanta [19] and Gao et al. [20].

Ho and Viskanta [21] reported basic heat transfer data during melting of *n*-octadecane on an isothermal vertical wall of a rectangular enclosure. The influence of natural convection currents on the melting rate and melting front profile were studied. Webb and Viskanta [22] studied the melting heat transfer of *n*-octadecane in an inclined rectangular enclosure. During the experiments the only recorded parameter was the interface shapes which were then used to infer the flow structures. It was found that decreasing the inclination angle increases the three-dimensionality of the flow field and results in non-uniform melting of the solid PCM.

Pal and Joshi [23] studied the melting of *n*-triacontane ($Pr \approx 31.8$) in a tall rectangular enclosure with one vertical side wall heated at a constant heat flux. They focused their attention on the effect of natural convection on the melting heat transfer. It was concluded that natural convection plays a dominant role during the initial stages of melting and its strength diminishes as it approaches full melting.

Shokouhmand and Kamkari [24] conducted experimental studies to visualize the interface evolution and temperature distribution during melting of lauric acid ($Pr \approx 100$) in a vertical rectangular enclosure. The thermophysical properties of lauric acid were determined and the role of natural convection heat transfer during different stages of melting was discussed.

Assis et al. [25] investigated the melting of RT27 ($Pr \approx 35$) in a spherical geometry. The study was concluded by both experimental measurements and numerical simulations. It was observed that melting in a spherical shell is accomplished by sinking of the solid in the liquid and close-contact heat transfer between the shell and solid PCM.

Tan [26] conducted an experimental study to compare constrained and unconstrained melting of *n*-octadecane in a spherical container. For constrained melting, the solid PCM is restrained from sinking. For unconstrained melting, the solid PCM is allowed to sink to the bottom of the sphere due to the gravity force. It was observed that during constrained melting, heat conduction only exists at the beginning of the melting process and at later times the dominant mode of heat transfer is natural convection in the liquid PCM. In unconstrained melting, the solid PCM sinks and melting at the bottom half accelerates due to the heat conduction at the lower part of the solid PCM. In another experimental and computational study, Tan et al. [27] investigated the role of buoyancy driven convection during constrained melting of paraffin wax ($Pr \approx 59.5$) inside a spherical capsule. Strong thermal stratification of the liquid PCM in the upper half of the sphere was observed. Also, fluctuation of measured temperature at the bottom of the sphere supported the establishment of chaotic flow structures which are responsible for waviness of the interface at the bottom of the solid PCM. Unconstrained melting of paraffin was also studied by Regin et al. [28] in a horizontal cylindrical capsule by visualizing the melting process. The result showed the important role of natural convection and close-contact melting during different stages of the melting process.

A major drawback of many prospective PCMs, especially the organic ones, is their low thermal conductivity ($k \approx 60 \text{ W}/\text{m K}$) which prevents rapid transfer of heat during heat storage (melting) and heat recovery (solidification). Therefore, heat transfer enhancement techniques are required for most latent heat thermal energy storage applications and thermal regulating systems. Different methods have been investigated to increase the thermal performance of PCMs, including using extended surfaces [29–33], impregnation of porous material [34–36], placement of high thermal conductivity metal structures [37,38], embedding heat pipe [39], dispersing high conductivity particles [40–42], adding carbon fibers [43,44] and carbon nanotubes [45,46] and utilizing dynamic melting [47]. Most of these enhancement methods rely on increasing the thermal conductivity of the PCM to augment the heat transfer rate. Considering that the melting rate in high Prandtl number PCMs is dominantly controlled by natural convection formed in the liquid PCM, any increase in the intensity of the natural convection currents can lead to considerable improvement of the melting rate. Using a fluid that is not a PCM in an enclosure, it has been proven that natural convection heat transfer is largely affected by the inclination angle of the enclosure [48]. The influence of the inclination angle on the thermal behavior and melting rate of PCM in an enclosure has been studied by few investigators. Akgun et al. [49] experimentally investigated the melting and solidification process

of paraffin in a vertical annular enclosure. It was found that the melting time can be decreased by 30% when the enclosure is tilted 5° from its vertical position. Sharifi et al. [50] investigated the effect of tilting during the outward melting from a vertical warm cylinder. Experiments were performed for small inclination angles of 5° and 10°. It was observed that modest tilting of the enclosure significantly affects the temperature distribution within the PCM, as well as the temporal evolution of the solid–liquid interface with a three-dimensional shape. This is a result of the interaction between 3D convection currents in the liquid PCM with the solid interface.

Recently, Baby and Balaji [51] experimentally evaluated the effect of orientation (0–120°) on the heat transfer enhancement of a porous matrix filled PCM based heat sink. A remarkable enhancement in heat transfer was obtained by placing the PCM in the porous matrix. However, the orientation of the heat sink did not show any significant impact on the heat sink performance. These results are attributed to the imposed restriction on development of the convection currents by small pores of the metal matrix and hence the dominant role of enhanced heat conduction.

The design of more practical and efficient thermal storage units and thermal regulating systems require a deeper understanding of the heat transfer mechanisms which govern the melting process of PCMs. Although many researchers have studied the role of natural convection during the melting process in different geometries as mentioned above, there is no detailed comparative study in the literature, of the effect of inclination angle on natural convection currents and melting rates in a rectangular enclosure. This paper investigates the heat transfer process and melting behavior during the solid–liquid phase change of lauric acid (as a high Prandtl number PCM) in a rectangular enclosure at different inclination angles. Qualitative and quantitative studies are performed by visualizing the solid–liquid interface patterns and temperature distribution within the enclosure. The present work uncovers the extent that the melting rate can be enhanced simply by inclining the enclosure.

2. Experiments

2.1. Test apparatus and procedure

An experimental apparatus has been designed and built to accurately measure the instantaneous solid–liquid interface evolution and temperature distribution within the PCM. The container was a rectangular enclosure with inside dimension of 50 mm in width, 120 mm in height and 120 mm in depth. The right wall of the enclosure was held at constant temperature using a heat exchanger. The other five walls of the enclosure were made of 25 mm thick transparent Plexiglass sheets to allow direct visualization and photography of the melting process and also to minimize the heat loss from the enclosure by their low thermal conductivity ($k = 0.17 \text{ W/m K}$). For additional insulation, the enclosure was insulated by 3 cm thick EPDM insulator sheets ($k = 0.042 \text{ W/m K}$). Fig. 1 shows a schematic view of the test cell. Thirty-two T-type thermocouples with a small wire diameter of 0.21 mm were placed at the vertical mid-plane of the enclosure to measure the transient temperature distribution within the enclosure (Fig. 2). Lauric acid with 99% purity (obtained from Panreac Chemical) was used as the PCM in this study. The thermophysical properties of lauric acid are listed in Table 1. In order to study the effect of inclination on the melting behavior of the PCM, the enclosure was mounted on an adjustable-tilt table.

Three sets of experiments were conducted for each inclination angles of 90°, 45° and 0° using three different wall temperatures of 70, 60, and 55 °C. All experiments were initiated by the solid PCM at a uniform temperature of 25 °C while the laboratory temperature was controlled at $25 \pm 1^\circ\text{C}$.

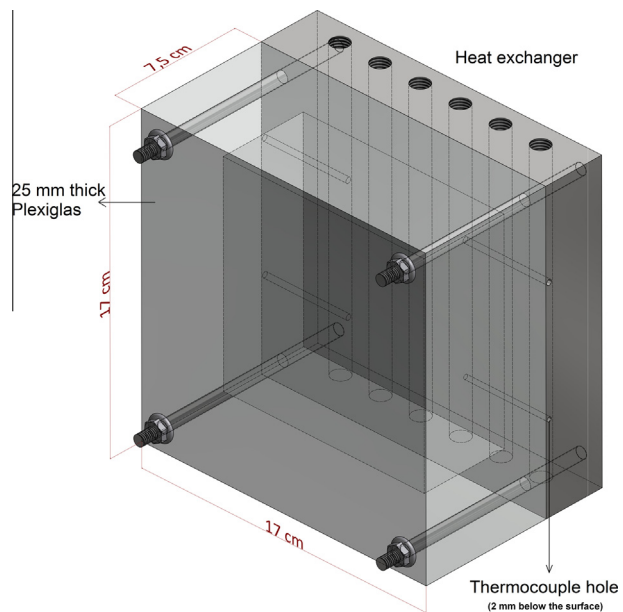


Fig. 1. Schematic view of the test cell (EPDM insulation of the enclosure is not shown in this figure).

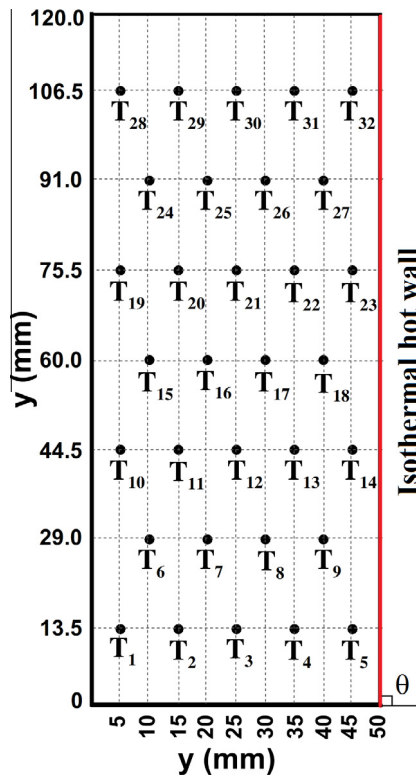


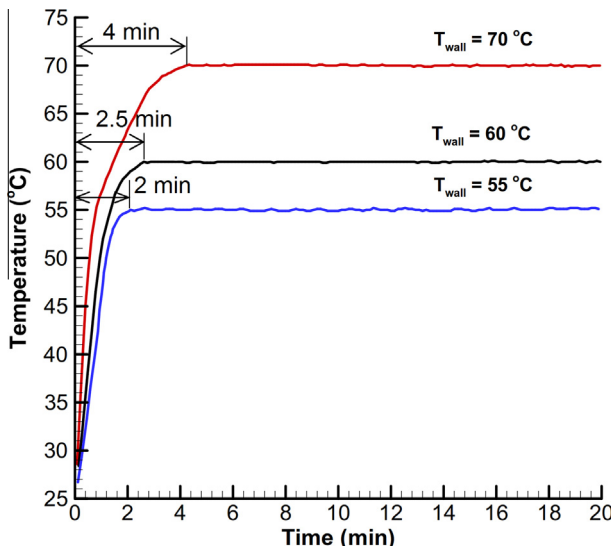
Fig. 2. Arrangement of thermocouples at the vertical mid-plane of the enclosure.

The experiments were started by circulating hot water at the desired temperature through the heat exchanger. Fig. 3 illustrates the time history of the average temperatures recorded on the surface of the heat exchanger. It can be seen that the hot wall temperature remains at a constant value within about 0.1°C after the initial transition. This figure only shows the first 20 min of the experiments to magnify the initial transition time. Since the experiments typically required from 2 to 9 h, the effect of the initial

Table 1

Thermophysical properties of lauric acid [24].

Specific heat capacity solid/liquid (kJ/kg K)	2.18/2.39
Melting temperature range (°C)	43.5/48.2
Latent heat of fusion (kJ/kg)	187.21
Thermal conductivity solid/liquid (W/m K)	0.16/0.14
Density solid/liquid (kg/m ³)	940/885
Kinematic viscosity (m ² /s)	6.7 × 10 ⁻⁶
Prandtl	100.7

**Fig. 3.** History of average temperatures on the surface of the heat exchanger.

transient period on the experimental results is deemed negligible. Further details of the experimental setup and test procedure are described in a previous paper [24].

2.2. Heat loss estimation

The experimental enclosure was designed to minimize the heat loss to the environment. Nevertheless, some heat is transferred to the surrounding by natural convection and radiation.

However, the radiation heat transfer can be neglected due to the low surface temperature of the insulation. Also, it should be mentioned that for visualizing the melt front, the insulation of the front face of the enclosure was being periodically removed. The photography was performed every 5 min for a time period of about 8 s. This means that the front insulation of the enclosure had been removed for about 2.5% of the total time of the experiment. So, total heat loss from the non-insulated wall of the enclosure was negligible.

In order to estimate the heat lost due to natural convection from the insulation surface, the temperatures of the insulation surfaces were measured by an infrared thermometer. The average Nusselt numbers on the vertical faces are estimated by Eq. (1) [52].

$$\overline{Nu}_v = 0.68 + \frac{0.67 Ra_v^{1/4}}{\left[1 + (0.492/\text{Pr})^{9/16}\right]^{4/9}} \quad (1)$$

The average Nusselt numbers on the top and bottom faces of the enclosure are estimated using Eqs. (2) and (3), respectively [53,54].

$$\overline{Nu}_t = 0.54 Ra_t^{1/4} \quad (2)$$

$$\overline{Nu}_b = 0.52 Ra_b^{1/5} \quad (3)$$

The Rayleigh number for the vertical surfaces is defined based on the height of the enclosure (L_v) while for the horizontal surfaces, the characteristic length (L_h) is defined as the ratio of surface area to its perimeter. The total heat loss from the enclosure can be calculated using the following equation:

$$Q_{\text{loss}} = \sum_{i=1}^{i=n} \frac{Nu_v k}{L_v} A_v \Delta T_i \Delta t_i + \sum_{i=1}^{i=n} \frac{Nu_t k}{L_t} A_t \Delta T_i \Delta t_i + \sum_{i=1}^{i=n} \frac{Nu_b k}{L_b} A_b \Delta T_i \Delta t_i \quad (4)$$

where ΔT_i is the temperature difference between the insulation surface and environment during the interval of Δt_i .

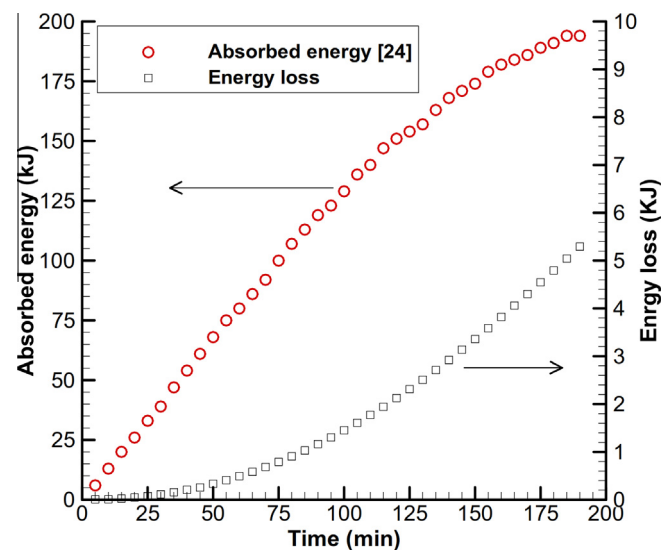
Fig. 4 compares the absorbed energy by the PCM with energy loss from the enclosure during the melting experiment with a hot wall temperature of 70 °C. As it can be seen, heat loss from the enclosure is negligible in comparison with the absorbed energy. The total heat loss is less than 2.7% of the total absorbed energy at the end of the melting process.

3. Results and discussions

3.1. Pattern of the solid–liquid interface

Visualizing the melting process reveals important flow patterns and dominant heat transfer mechanisms during the solid–liquid phase change of the PCM. Fig. 5 shows the sequential photographs of the melting process at different inclination angles of 90°, 45° and 0° when a uniform temperature of 70 °C is imposed on the right wall of the enclosure. Lauric acid in the solid phase has an opaque white color which transforms to a transparent liquid upon melting. So, in these photographs, white and black areas represent the solid and liquid phases, respectively.

Fig. 5(a)–(e) visualizes the melting process in the vertical enclosure ($\theta = 90^\circ$). During the initial period of melting ($t \leq 10$ min), a thin layer of melted PCM appears adjacent to the hot wall, indicating that the heat transfer mechanism is predominantly by conduction. This mode of heat transfer prevails as long as the viscous force opposes the fluid motion during which the solid–liquid interface remains almost uniform and parallel to the hot wall. As time progresses and the melt layer thickness increases, the buoyant force becomes large enough to overcome the viscous force. At this stage,

**Fig. 4.** A comparison between the absorbed energy and heat lost from the enclosure during the melting process in vertical enclosure with hot wall temperature of 70 °C.

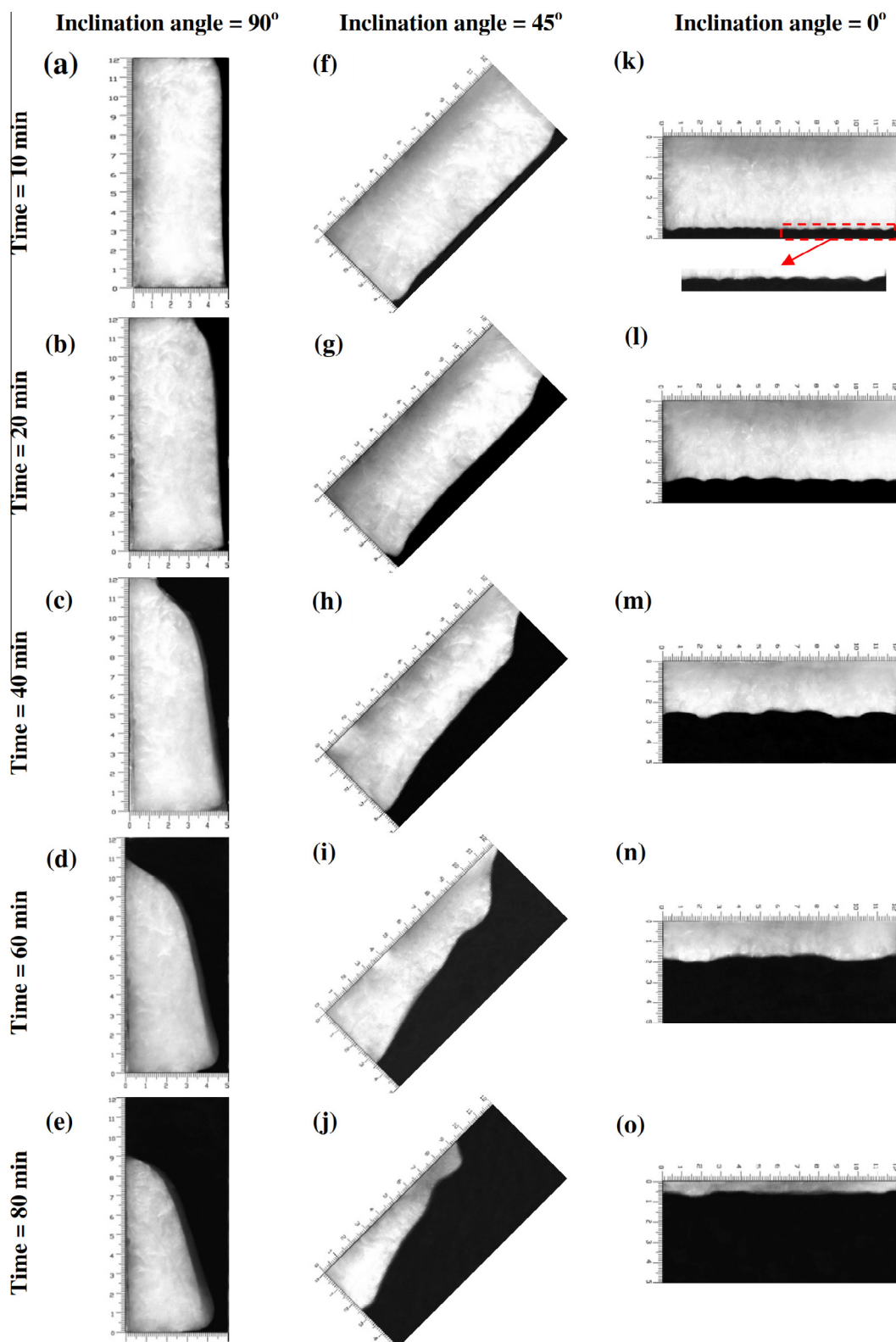


Fig. 5. Sequential photographs of the melting process of PCM in the rectangular enclosure for different inclination angles with hot wall temperature of 70 °C.

a natural convection current is initiated in the melt region which presents itself by eroding the top part of the solid–liquid interface (Fig. 5(a)). The development of buoyant force results in the formation of a growing circulating current in the top part of the enclosure creating a concave curvature at the top of the melt front while in the lower part of the cavity, the interface is linear and

the tilt increases with time (Fig. 5(b) and (c)). A continuous change in the melt layer thickness and regular change in the shape of the solid–liquid interface indicates the formation of a dominant circulating current in the liquid PCM. At later times (Fig. 5(d) and (e)), the melt front reaches the opposite side wall and the shape of the interface at the upper part of the solid PCM changes from a

concave curvature to a convex curvature. This pattern of melting continues until the solid PCM melts completely.

Fig. 5(f)–(j) visualizes the melting process in the enclosure with an inclination angle of 45°. Unlike **Fig. 5(a)** which shows a very thin melt layer, especially at the lower part of the cavity, **Fig. 5(f)** shows a thicker melt layer at the lower part of the enclosure. This difference reveals that the transition from conduction-dominated to natural convection-dominated melting occurs earlier, as evidenced by the slight concavity in the solid–liquid interface and higher melting rate than that of **Fig. 5(a)**. As time progresses, concavity of the interface becomes more pronounced (**Fig. 5(g)** and (**h**)). This discrepancy in the shape of the interface at the lower part of the enclosure, between inclination angles of 45° and 90°, implies the presence of different flow structures in the liquid PCM. The flow structures in the 45°-inclined enclosure can be explained as follows: the liquid PCM is heated up on the hot wall, and rather than rising parallel to the hot wall as in the vertical case, it separates from the hot wall and impinges to the solid interface which results in a higher melting rate and produces a higher curvature in the solid–liquid interface. At later times (**Fig. 5(i)** and (**j**)), unusual and non-uniform shapes were observed at the solid–liquid interface. These irregularities are attributed to the three-dimensional flow structures and vortex motions in the liquid PCM [22].

Fig. 5(k)–(o) visualizes melting from the bottom in the horizontal enclosure ($\theta = 0^\circ$). At the very early stages of melting, the solid–liquid interface is nearly flat and heat conduction is the dominant mode of heat transfer. Later, the interface shape becomes wavy and is controlled to a large extent by complex convection currents in the liquid PCM (**Fig. 5(k)**). The wavy shape of the interface can be referred to as the formation of three-dimensional Benard convection cells in the liquid PCM which leads to a non-planar, hexagonal capped solid–liquid interface. In each Benard convection cell, the hot liquid PCM rises vertically away from the hot wall in the central region of the cell and after impingement to the interface and eroding the solid PCM falls around the edges of the cell. The effect of three-dimensional flow structures on the waviness of the bottom interface has also been observed by other investigators [19,20,27]. It can be noticed that the number of convection cells is proportional to the melt layer thickness. As melting progresses (**Fig. 5(l)** and (**m**)), the convection cells merge with neighboring ones and become larger while the uniformity of size distribution of the cells diminishes. This may be due to the turbulent natural convection appearing in the liquid PCM [55]. Towards the end of the melting process (**Fig. 5(n)** and (**o**)), the convection cells join and the flow structure seems to change to nearly two-dimensional convection rolls [55]. This is evident from a decrease in both the number and sharpness of the corrugations at the solid–liquid interface.

Fig. 6 shows the solid–liquid interface at various times during the melting process for different inclination angles of 90°, 45° and 0° with different hot wall temperatures of 70 °C, 60 °C and 55 °C. It can be observed that the interface pattern is greatly influenced by the inclination angle of the enclosure while the effect of the decrease in hot wall temperatures is only to delay the development of the interface. There are no distinct changes in the shape of the interfaces with varying hot wall temperature in the range of 55–70 °C ($3.6 \times 10^8 \leq Ra \leq 8.3 \times 10^8$) which implies that the main flow structures in the liquid PCM appear to be almost identical. If one compares **Fig. 6(a)** with **Fig. 6(c)**, it can be seen that after 10 min from the start of the experiments, the initiation of convection current has been postponed by decreasing the hot wall temperature from 70 °C to 55 °C. This is concluded from the curved interface of **Fig. 6(a)** and the flat interface of **Fig. 6(c)** after 10 min from the start of the experiments. There are similar explanations for the inclination angles of 45° and 0°.

Visual observations confirmed that during the melting process in the vertical enclosure there is no change in shape of the

solid–liquid interface along the direction normal to the viewing plane. This indicates that natural convection flow in the liquid PCM remains two-dimensional during the whole melting process. However, as the inclination angle decrease to 0°, the interface becomes wavy and irregular as a result of the formation of 3D convection currents in the liquid PCM.

3.2. Temperature distribution

For qualitative presentation of the temperature distribution in the enclosure, Tecplot software was used for post-processing of the recorded temperatures based on the linear interpolation of the temperatures. **Fig. 7** provides further illustration, showing temperature contours at the vertical mid-plane of the enclosure for different inclination angles with the hot wall temperature of 70 °C at different times of the melting process.

Fig. 7(a)–(e) shows the constant temperature profiles in the vertical enclosure. During the early period of melting (**Fig. 7(a)**), temperature contours are nearly parallel to the hot wall indicating that heat is transferred in the normal direction to the hot wall and heat conduction is the dominant mode of heat transfer. It should be noted that the corrugated shape of contours is due to the staggered arrangement of the thermocouples. Later (**Fig. 7(b)** and (**c**)), the temperature of the liquid PCM adjacent to the hot wall increases sufficiently enough so that the buoyant force overcomes the viscous force and hot liquid PCM rises along the vertical hot wall. When the hot liquid PCM reaches to the top wall of the enclosure, it is deflected towards the solid PCM. Impingement of the hot liquid PCM to the solid–liquid interface accelerates the local heat transfer and consequently the melting rate. **Fig. 6(a)** shows that the rate of melting at the lower part of the enclosure is much less than that of the upper parts. This can be explained by the fact that the temperature of the hot liquid PCM decreases as it descends along the interface and results in less heat transfer to the solid PCM at the lower parts of the enclosure. As the solid PCM shrinks and its peak point moves down along the left wall of the enclosure (**Fig. 7(d)** and (**e**)), the temperature of the liquid PCM at the upper part of the enclosure (the region above the peak point of the solid PCM) increases which confirms the presence of the weak velocity field at this part of the liquid PCM. Furthermore, accumulation of the hot liquid PCM at the upper part of the enclosure reveals that a considerable portion of the heat absorbed by the liquid PCM from the hot wall is directed to the upper part of the enclosure where there is no solid PCM. In this region, hot liquid PCM sits on the cold heavier liquids layers resulting in the development of stratified liquid layers.

Fig. 7(f)–(j) illustrates the temperature contours in the 45°-inclined enclosure. When these contours are compared with those of the vertical enclosure (**Fig. 7(a)–(e)**), it can be seen that unlike the vertical case, stratified temperature layers do not appear at the upper part of the enclosure. This means that most of the absorbed heat by the liquid PCM is transferred to the solid PCM, increasing the melting rate.

Fig. 7(k)–(o) shows the temperature contours in the enclosure during melting of the PCM from below. In comparison with the two other cases (90° and 45°-inclined enclosures), the temperature of the liquid PCM is almost uniform throughout the melting process. The uniformity of the temperature distribution along with the waviness of the interface observed in **Fig. 7(k)–(o)** discloses the presence of the vortical flow structures in the liquid PCM which are responsible for efficient energy transport from the hot wall to the solid–liquid interface and mixing the liquid PCM.

Fig. 8 shows the temperature distributions in the vertical mid-plane of the enclosure measured from two different thermocouple rows (first and seventh) for a hot wall temperature of 70 °C. For all inclination angles, the time period in which the temperature

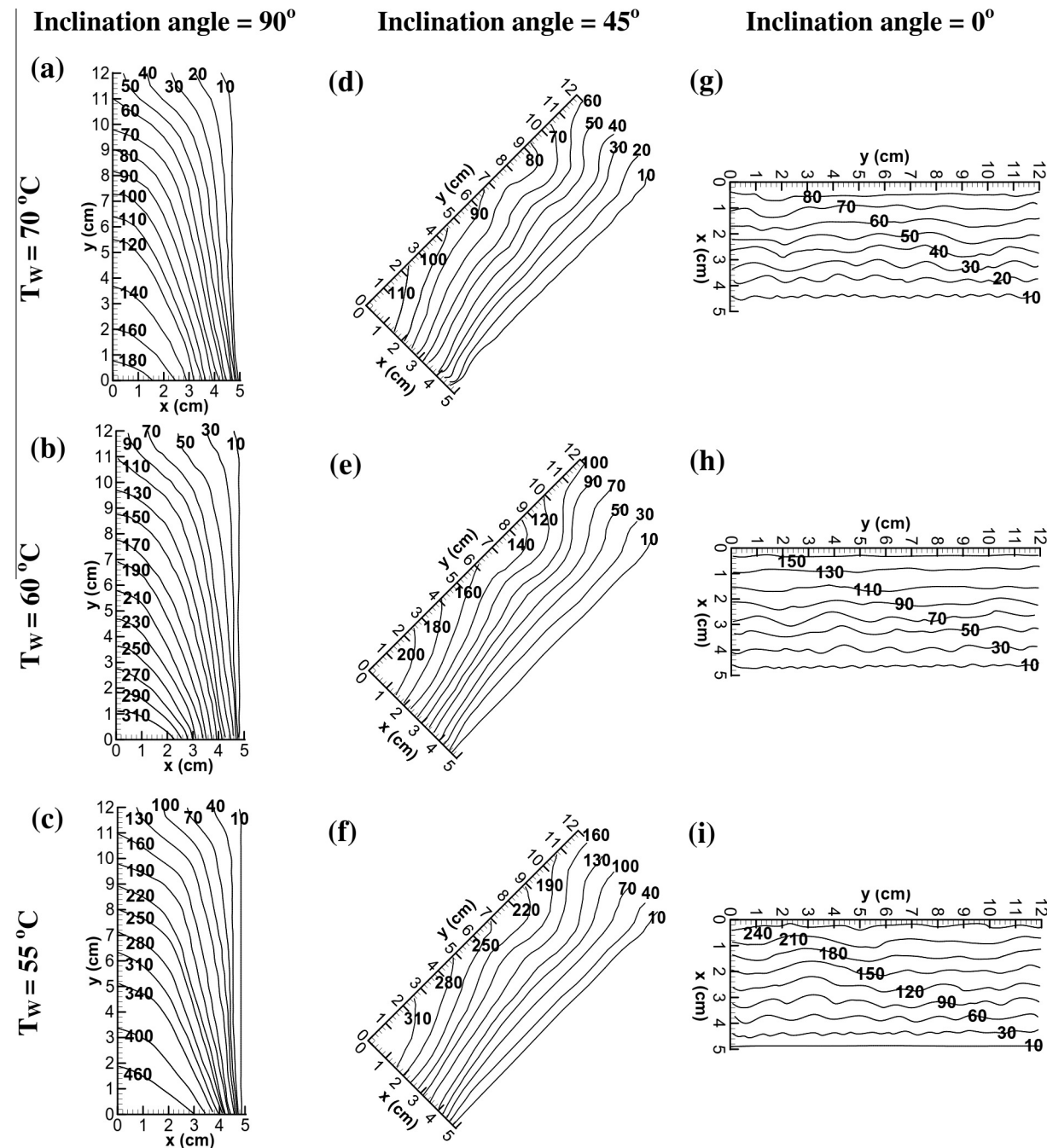


Fig. 6. Solid-liquid interface progress during the melting of PCM in the rectangular enclosure with different inclination angles and different hot wall temperatures (numbers on the interfaces represent the minutes passed from the start of the melting process).

distributions are placed below the melting temperature line ($T_m = 43.5^\circ\text{C}$) is associated with the conductive heating of the solid PCM. As expected, by the time the heat conduction is the dominant mode of heat transfer at the lower and upper part of the enclosure, the temperature distributions are the same at both thermocouple racks. At any given time, this figure can be used to estimate the interface position at each thermocouple row without the need to directly visualize the melting process. The interface position corresponds to the point that the temperature distribution intersects the melting line.

For the vertical enclosure (Fig. 8(a) and (b)), when the melt front passes the seventh row of the thermocouples (Fig. 8(b)), large temperature changes are observed. Temperature changes are smaller as the melt front passes the first row of thermocouples

(Fig. 8(a)). The value of the temperature change can be an indicator of the strength of the local heat transfer rate on the solid–liquid interface at different heights of the enclosure. A larger temperature change indicates the existence of a thinner thermal boundary layer, and consequently a greater local heat transfer rate on the interface at the upper part of the enclosure in comparison with lower part.

As explained before, the convection current in the liquid PCM is the result of temperature gradients between the right wall of the enclosure (hot source) and moving solid–liquid interface (cold source). As the melt front touches the opposite wall of the enclosure and disappears from the upper parts of the enclosure, the temperature gradient as the source of the convection current diminishes and the convection current is weakened in this region. It is evident from Fig. 8(b) that during the time interval of

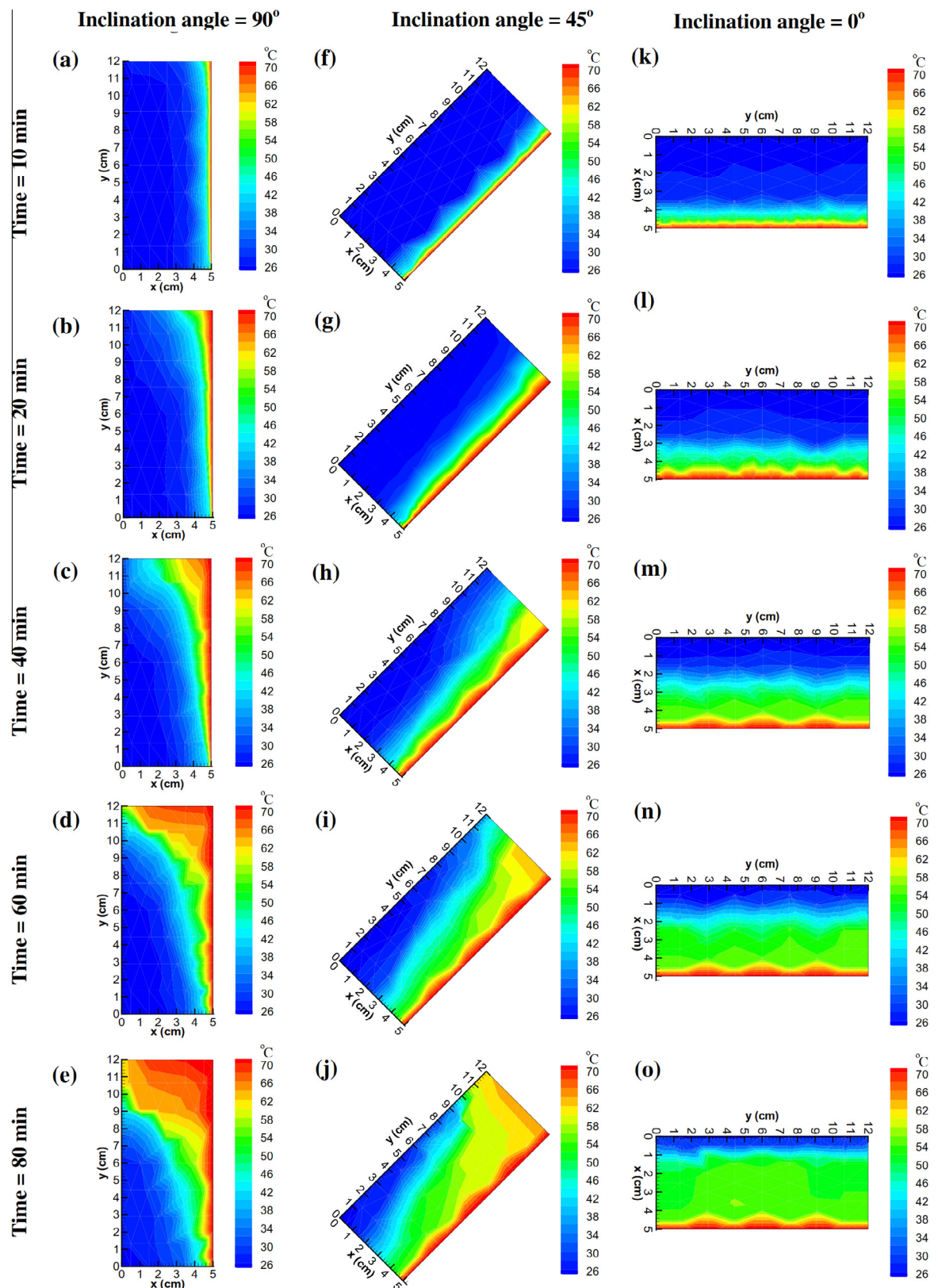


Fig. 7. Instantaneous temperature contours at the vertical mid-plane of the enclosure with different inclination angles when hot wall temperature is 70 °C.

110–190 min, almost uniform temperature distributions are observed at the seventh row of the thermocouples. The time-independent uniform temperature distribution at the upper part of the enclosure implies the presence of negligible convection currents in

this region of the enclosure. The same explanation can be applied for the 45°-inclined enclosure (Fig. 8(c) and (d)). In the 45°-inclined enclosure, when the melt layer thickness increases, the thermocouples placed in the liquid PCM show a uniform temperature

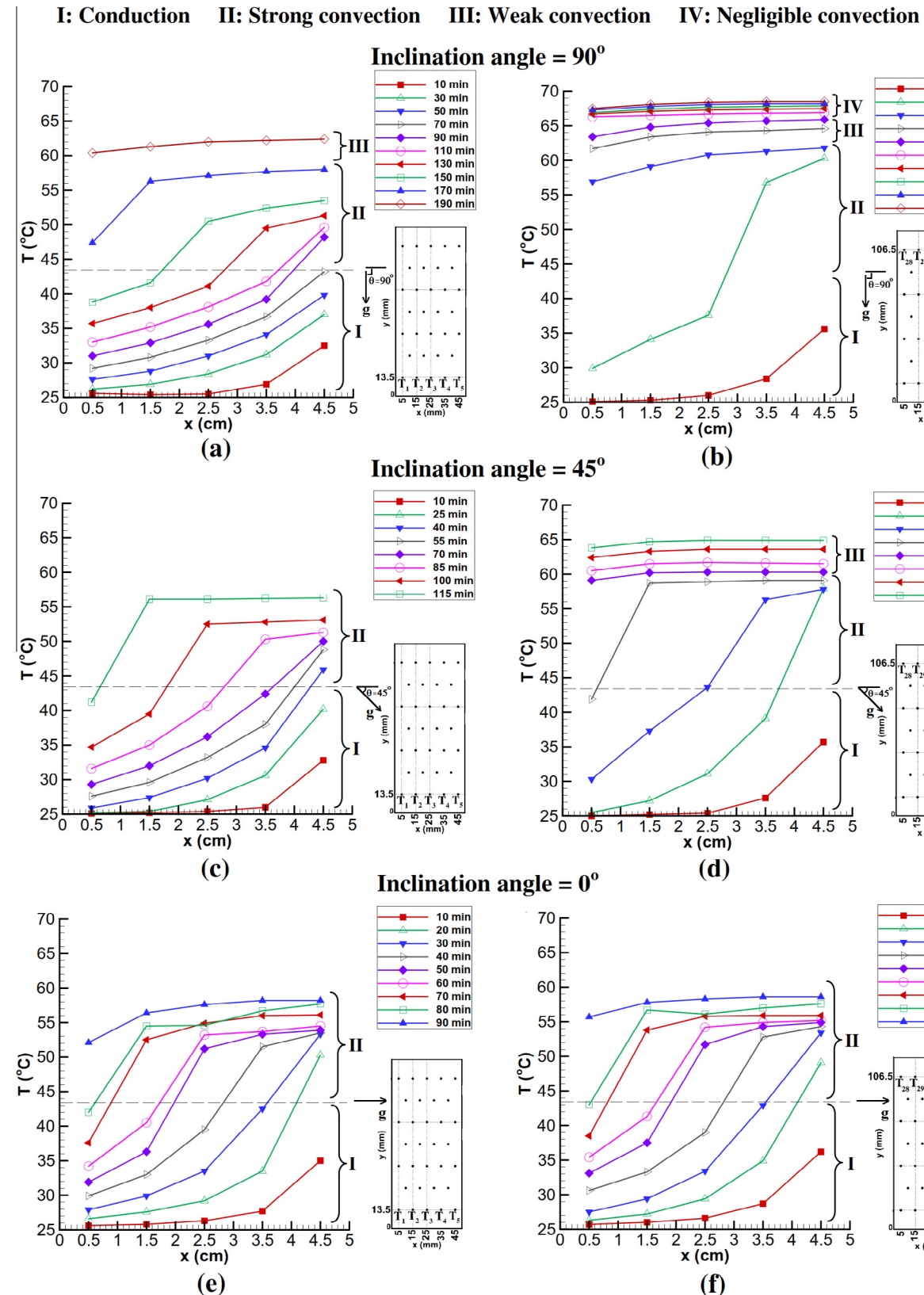


Fig. 8. Temperature distributions at the vertical mid-plane of the enclosure with a hot wall temperature of 70 °C for different inclination angles.

distribution while in the vertical enclosure, small temperature gradients exist in the liquid PCM. This denotes that, contrary to the 45°-inclined enclosure, heat conduction, in normal direction to the hot wall, could play a role during the heat transfer in the liquid

PCM of the vertical enclosure although the convection is still the dominant mode of heat transfer.

During melting from below (Fig. 8(e) and (f)), temperature distributions at the first and seventh rows of the thermocouples show

nearly similar trends with small discrepancies regarding to three-dimensionality and asymmetrical nature of the convective flow structures in the liquid PCM.

3.3. Temperature history

The temperature history of the thermocouples provides more accurate information needed to investigate the effect of inclination angle on the thermal behavior and kinetics of the melting process.

Fig. 9 shows the temperature histories of the first and fifth columns of the thermocouples for different inclination angles of the enclosure when the hot wall temperature is maintained at 70 °C. For all inclination angles, initially the temperature of the thermocouples increases due to heat conduction in the solid PCM until the melting temperature is reached. During this period of time, the rate of temperature increase of the first column of thermocouples is much higher than those of the fifth column. This can be explained by the fact that the heat transfer to the solid PCM surrounding the first column of thermocouples is by strong heat conduction through the thin layer of the liquid PCM (less than 5 mm thick). It should be emphasized that the conduction mode of heat transfer over convection is only limited to the thin layer of liquid PCM. This is similar to the high melting rate during close contact melting of PCM in a spherical enclosure [26].

For the vertical enclosure (Fig. 9(a)), sharp increases in temperatures are observed as the thermal boundary layer associated with

the melt front passes each thermocouple, and then the temperatures increase slightly until the end of the melting process. Attention is focused on the different values of temperature increase when the melt front passes the thermocouples. The thermocouples placed at the higher part of the enclosure (e.g., T₃₀ and T₃₂) experience higher temperatures than those of the lower part of the enclosure (e.g., T₃ and T₅). At the end of the sharp temperature increase, thermocouples at the first column T₃₂, T₂₃, T₁₄ and T₅ reach the temperatures of 58.5, 52.5, 51 and 47.5 °C, respectively. These temperatures are associated with the temperatures of the liquid PCM at the edge of the thermal boundary layer. The decreasing trend of temperatures from the upper to lower thermocouples implies the thickening of the thermal boundary layer along the interface and confirms the presence of a counter-clockwise rotating flow in the liquid.

The temperature histories of the 45°-inclined enclosure (Fig. 9(b)), show almost identical trends to those of the vertical enclosure, except some minor fluctuations in temperature of the first column of thermocouples which are attributed to three-dimensional and unstable flow structures in the liquid PCM. The presence of three-dimensional flow structures in inclined enclosure were also reported by Webb and Viskanta [22] through the observation of the solid–liquid interface morphology and by Sharifi et al. [50] during the melting of PCM in a cylindrical enclosure with small tilt angles. As evident from temperature history of the fifth column of thermocouples, temperature fluctuations are

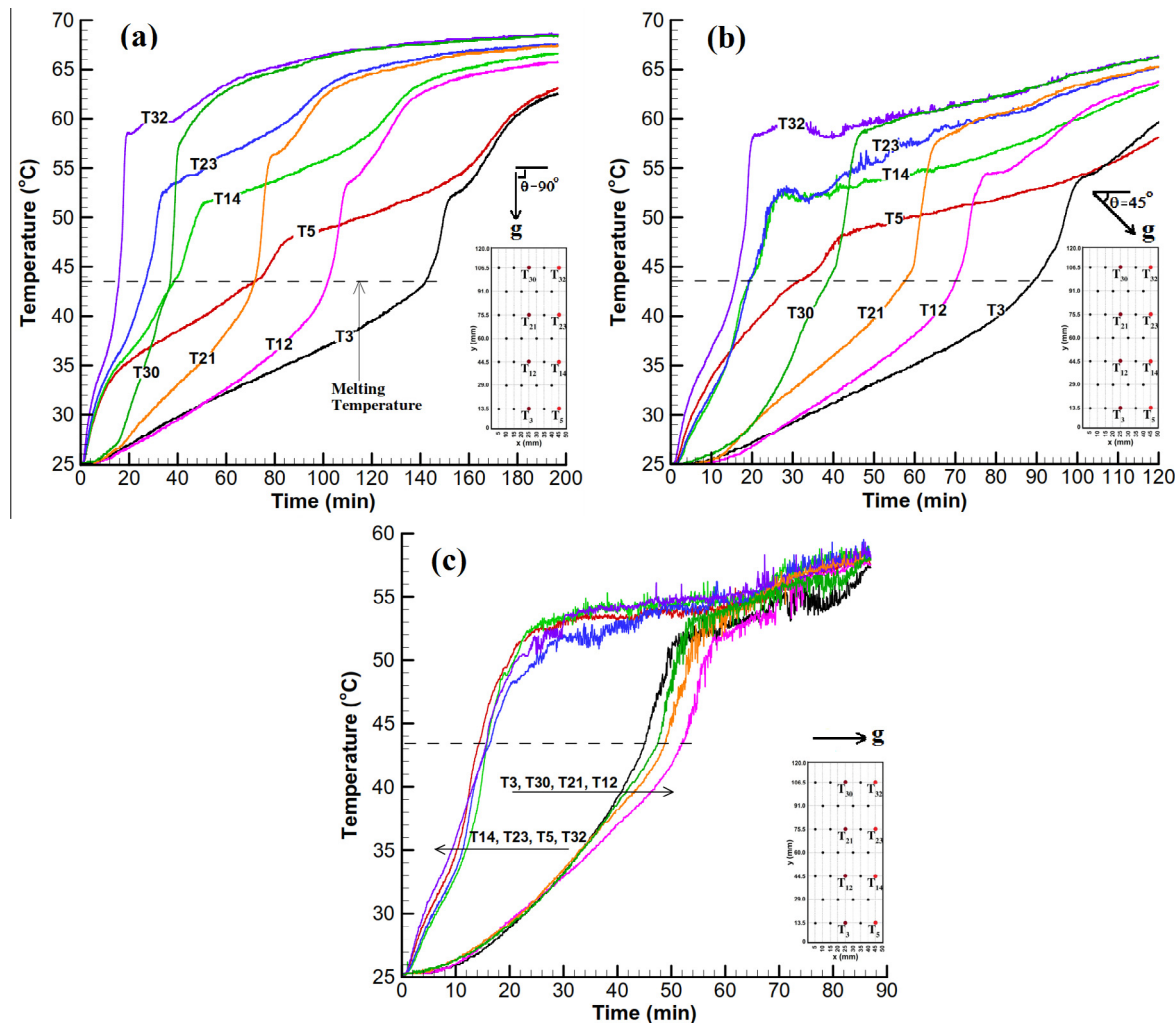


Fig. 9. Temperature history of the first and fifth columns of thermocouples during melting of PCM in the enclosure with hot wall temperature of 70 °C: (a) $\theta = 90^\circ$, (b) $\theta = 45^\circ$, and (c) $\theta = 0^\circ$.

diminished when the melt thickness increases. This might be due to the weakening of three-dimensional flow structures in the liquid PCM.

During melting from below (Fig. 9(c)), temperatures of the thermocouples adjacent to the hot wall (T_5, T_{14}, T_{23} and T_{32}) increase almost uniformly, with no significant fluctuations, as the melt front pass them while the thermocouples placed at a further distance (T_3, T_{12}, T_{21} and T_{30}) show fluctuating temperatures immediately after the melt front touches them. This thermal behavior is attributed to regular convection cells in the thin melt layer and development of turbulent convection currents in the thick layer of the melted PCM. Similar temperature behaviors were reported by Gau et al. [20] with thermocouples located at 2.8 and 28 mm above the heated plate.

It can be observed that the mean temperature of thermocouples converges approximately to the same value, soon after they are placed in the bulk of the liquid PCM. As mentioned before, the uniformity of the temperature of the liquid PCM is the result of the

vortical and chaotic flow structures distributed in the bulk of the liquid PCM.

Observing the instantaneous variation of maximum temperature within the enclosure gives more knowledge about the heat transfer and thermal behavior of the PCM during the melting process in the inclined enclosure. For this purpose, the maximum temperature readings among all 32 thermocouples were found at every time step (2 s) during the whole melting process. Fig. 10 shows the maximum temperature variations within the enclosure with a hot wall temperature of 70 °C for different inclination angles. It clearly shows that the reduction in inclination angle from 90° to 0° decreases the maximum temperature of the liquid PCM and increases the temperature fluctuations. A decrease in temperature of the liquid PCM leads to an increase of temperature gradient between the hot wall and bulk of the liquid PCM and hence more heat transfer from the hot wall to the liquid PCM and a faster melting rate can be achieved. Also, increasing the inclination angle contributes to thermal storage of the PCM by increasing the sensible heating of the liquid PCM. These findings can be useful for the application of PCM to the thermal control of electronic components where the maximum temperature rise of the components is important.

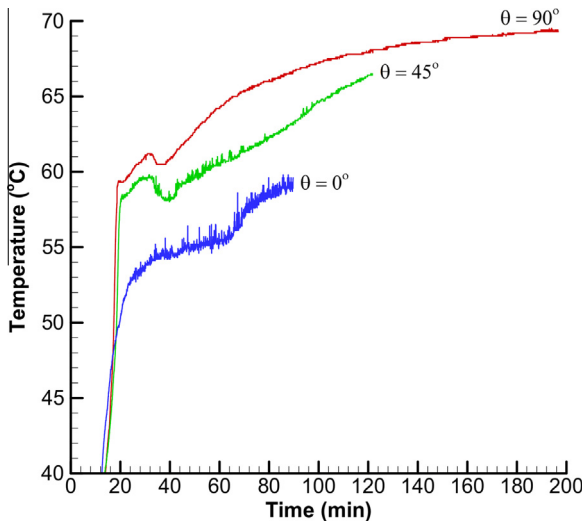


Fig. 10. Variation of maximum temperature versus time within the enclosure with hot wall temperature of 70 °C and different inclination angles.

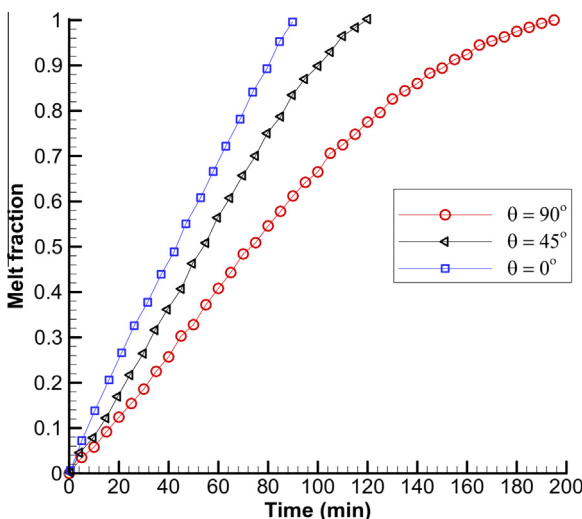


Fig. 11. Comparison of the melt fraction variations versus time for different inclination angles of the enclosure with hot wall temperature of 70 °C.

3.4. Heat transfer characteristics

3.4.1. Melting rate

Fig. 11 compares the melt fractions in the enclosure for different inclination angles at every five minutes while the hot wall temperature was maintained at 70 °C. For all inclination angles, melt fractions increase almost linearly with time. As the solid PCM shrinks

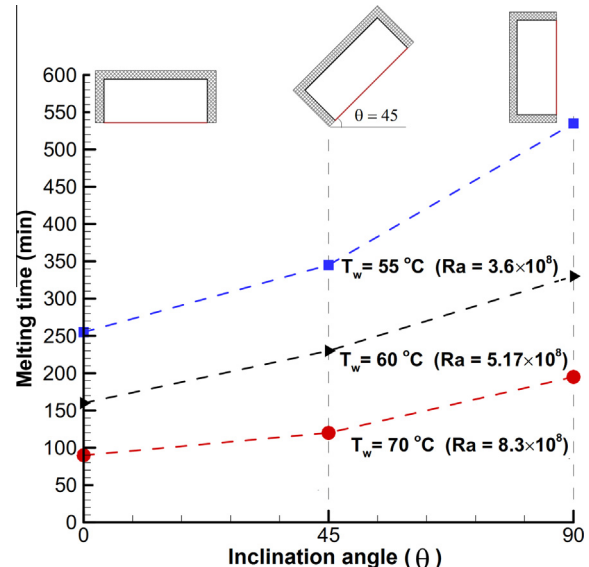


Fig. 12. Variation of total melting time versus inclination angle for different wall temperatures.

Table 2
Melting time ratios for different experiments.

Hot wall temperature (°C)	Melting time ratio			
	Inclination angle	90°	45°	0°
70		1	0.62	0.46
60		1	0.68	0.48
55		1	0.65	0.47

in the vertical enclosure, melt fraction variations deviate from a linear trend and the melting rate decreases because of suppression of the convection current while for the horizontal enclosure, melt fractions vary linearly with time until the end of the melting

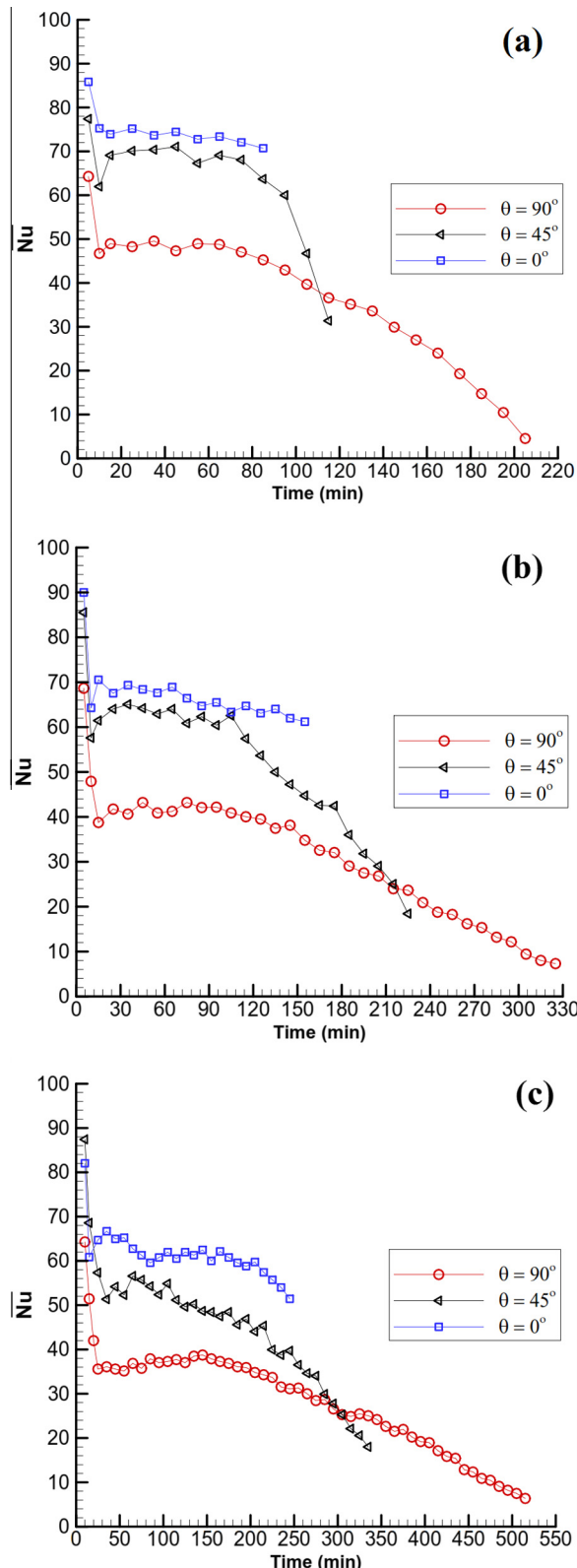


Fig. 13. Comparison of surface-averaged Nusselt number variations versus time for different inclination angles of the enclosure and different hot wall temperatures: (a) $T_w = 70^\circ\text{C}$, (b) $T_w = 60^\circ\text{C}$, and (c) $T_w = 55^\circ\text{C}$.

process. This means that during melting in the enclosure from the bottom, no significant reduction in the heat transfer rate occurs. This result reveals that when melting from the bottom, the heat transfer rate of a high Prandtl number PCM is not affected by the melt layer thickness during the phase change process.

Similar melting trends were obtained for hot wall temperatures of 60 and 55°C .

Fig. 12 shows the total melting time versus inclination angle for different wall temperatures. It clearly illustrates that the melting time decreases as the inclination angle is reduced. This remarkable decrease in melting time is attributed to an increase of vortical and chaotic flow structures in the liquid PCM when the inclination angle is decreased.

Table 2 summarizes the melting time ratios for different hot wall temperatures and inclination angles. The melting time ratio is defined as the ratio of the melting time of the PCM in the inclined enclosure to the melting time in the vertical enclosure. It is found that the melting time in the horizontal enclosure is less than half of that in the vertical enclosure. It is interesting to note that the melting time in the vertical enclosure with a hot wall temperature of 70°C is 22% more than that in the horizontal enclosure with a lower temperature of 60°C . This shows that, despite the decrease in hot wall temperature, the prevailing effect of the inclination angle increases the heat transfer rate and decreases the melting time.

3.4.2. Nusselt number

Surface Nusselt numbers have been calculated for all experiments and the results are compared in Fig. 13. The surface-averaged Nusselt number can be expressed as [24]:

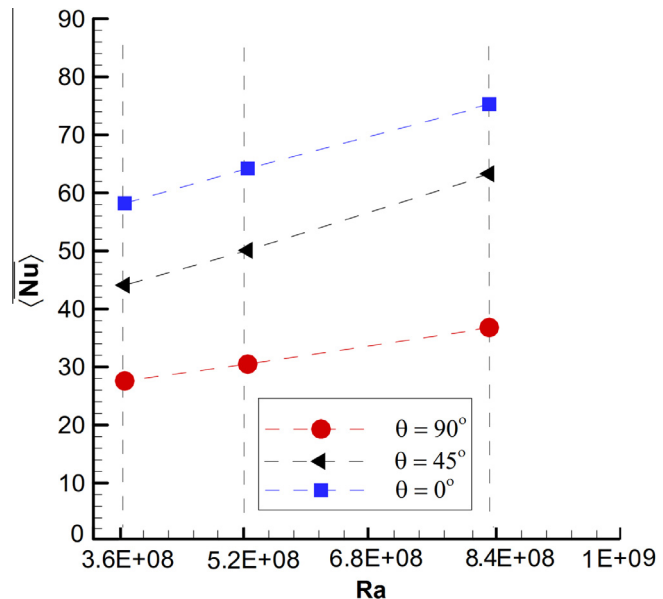


Fig. 14. Variation of the time-averaged Nusselt number with Rayleigh number for different inclination angles.

Table 3
Nusselt number enhancement ratios for different experiments.

Hot wall temperature ($^\circ\text{C}$)	Nusselt number enhancement ratio			
	Inclination angle	90°	45°	0°
70		1	1.72	2.05
60		1	1.64	2.1
55		1	1.60	2.11

$$\bar{Nu}(t) = \frac{\bar{h}(t)H}{k_l} \quad (5)$$

The characteristic length is taken to be the height of the vertical enclosure (H) [20,56–59]. For the sake of comparison of Nusselt numbers relating to inclined enclosures with the vertical enclosure, the same length scale is considered for the other inclination angles.

Variations of Nusselt numbers with time can be used to identify the different heat transfer mechanisms governing the melting process in the enclosure. For all inclination angles and hot wall temperatures, Nusselt numbers start with relatively large values at the initiation of the heat transfer process and drop very rapidly during the conduction regime. The initial large Nusselt numbers are attributed to the small thermal resistance of the very thin liquid layers at the start up time which accordingly increases the heat transfer rates. At the end of the conduction regime, Nusselt numbers experience local minimum values and then increase slightly which show the formation of convection currents in the liquid PCM and enhancement in the heat transfer rate. After the short period of transition from conduction to convection, Nusselt numbers show quasi-steady values representing the convection dominated stage of melting. It is obvious from Fig. 13 that the highest value of quasi-steady Nusselt number is related to the 0° -inclined enclosure and reduces by increasing the inclination angle. It can be observed that during melting of the PCM from the bottom, the quasi-steady Nusselt number persists until the end of the melting process while for the 45° and 90° -inclined enclosures, after the time period of quasi-steady heat transfer, Nusselt

numbers decrease with time. This reducing trend indicates the weakening of convection currents caused by the increase in the bulk temperature of the liquid PCM and decrease in the length of the solid–liquid interface. The interface acts as the cold source for driving the natural convection currents in the enclosure. Unlike melting in the 90° and 45° -inclined enclosures, during melting in the 0° -enclosure, the length of the interface was almost constant and strong convection currents persist to the end of the melting process. Therefore, no significant decrease in Nusselt number can be observed during melting of the PCM from below. It can be concluded that in the range of the Rayleigh numbers considered in this study, the melting heat transfer rates are not affected by the thickness of the liquid layer.

Fig. 14 shows the variation of the time-averaged Nusselt number with Rayleigh number for different inclination angles. The time-average Nusselt number is defined as the average of surface-averaged Nusselt number over the whole melting time (t_{total}) calculated as follows:

$$\langle \bar{Nu}(t) \rangle = \frac{1}{t_{total}} \int_0^{t_{total}} \bar{Nu}(t) dt \quad (6)$$

As observed, the Nusselt number increases linearly with an increase of Rayleigh number and the highest value of Nusselt numbers are attributed to the heat transfer when melted from below.

Table 3 shows Nusselt numbers enhancement ratios for different hot wall temperatures and inclination angles. The Nusselt number enhancement ratio is defined as the ratio of time-averaged Nusselt

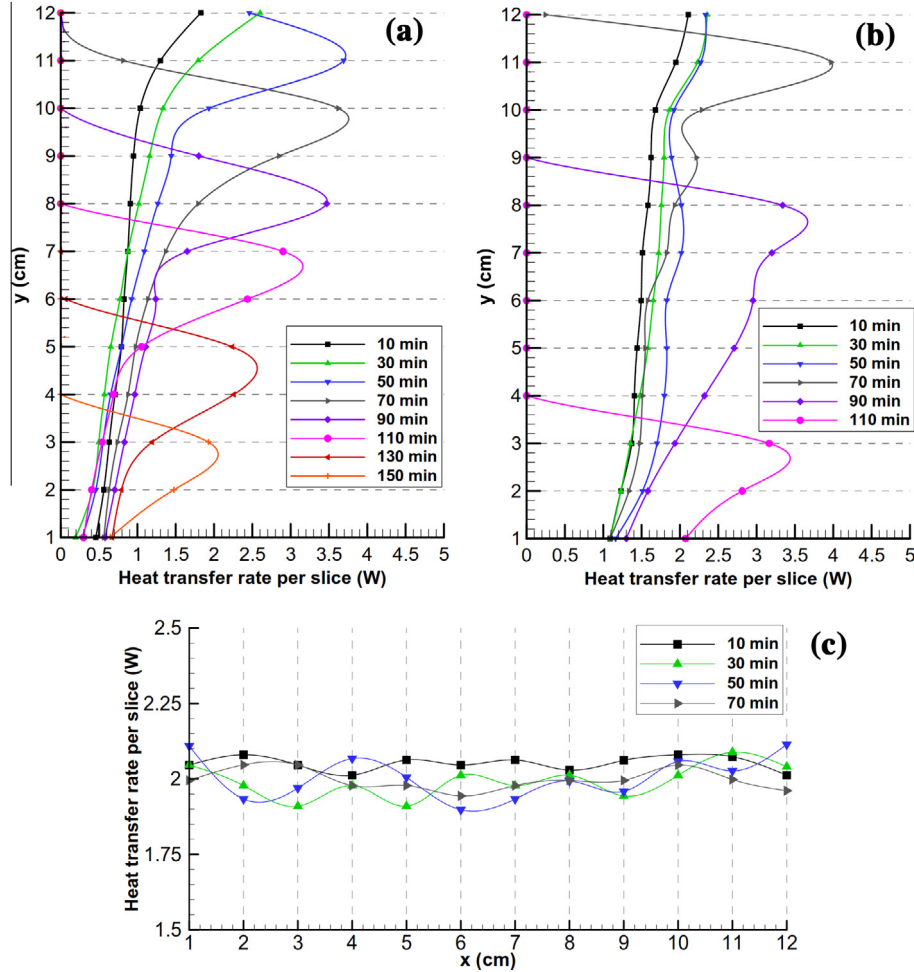


Fig. 15. Solid–liquid interface heat transfer rates during melting of PCM in the enclosure with hot wall temperature of $70\text{ }^\circ\text{C}$: (a) $\theta = 90^\circ$, (b) $\theta = 45^\circ$, and (c) $\theta = 0^\circ$.

Table 4

Maximum value of uncertainties for different variables.

Variable	Maximum value of uncertainty		
	Inclination angle	90° (%)	45° (%)
Melt fraction	±2.9	±2.3	±2.1
Nusselt number	±12.8	±11.3	±9.2
Interfacial heat transfer	±6.4	±5.3	±2.5

number in the inclined enclosure to that of the vertical enclosure. As expected, for each inclination angle, the time-averaged Nusselt number reduces with decreasing hot wall temperature. Nusselt number enhancement ratios increase, even more than two times, with a decrease of inclination angles from 90° to 0°.

3.4.3. Local interfacial heat transfer rate

In order to expand the understanding of the interfacial heat transfer process during melting of PCM in inclined rectangular enclosures, the local interfacial heat transfer rates have been calculated for every 20 min and results for the hot wall temperature of 70 °C are presented in Fig. 15. At the early stages of melting in the 90° and 45°-inclined enclosures (Fig. 15(a) and (b)), the local heat transfer rates are almost uniform except at the upper part of the enclosure which is consistent with the initial heat conduction at the lower part of the enclosure and formation of convection current at the upper part. As the convection currents are intensified, the interfacial heat transfer rates at the upper and lower part of the 45°-inclined enclosure are enhanced while for the 90°-inclined enclosure this enhancement is only observed at the upper part. When the melt front reaches the opposite wall, the heat transfer distribution shows a maximum value corresponding to the top of the solid PCM and zero values represent the slices with totally liquid PCM. As melting progresses and the solid PCM shrinks, the peak values of heat transfer curves decrease and the number of slices with zero heat transfer increases.

During melting from below (Fig. 15(c)), the local heat transfer rates along the interface exhibit a nearly periodic variation. This a clear indication of the development of multiple vortex circulation pattern in the liquid PCM. Also, the averaged values of interfacial heat transfer rates at any times are almost the same and no abrupt changes are observed in heat transfer rate distribution which is in agreement with the quasi-steady Nusselt numbers depicted in Fig. 13.

4. Uncertainty analysis

The uncertainties of experimental results are always influenced by inevitable errors occurring in the experimental measurements and depend on the uncertainty of the individual measuring instruments. Based on the uncertainty analysis method of Kline and McClintock [60], propagation of uncertainty in the final result is affected by the uncertainties of independent variables. This method is employed to estimate the uncertainties of experimental results. The maximum uncertainties of melt fraction, Nusselt number and interfacial heat transfer are calculated for different inclination angles and the results are shown in Table 4.

5. Conclusion

An experimental investigation was conducted to examine the effect of inclination angle on the thermal characteristics of the melting process in a rectangular enclosure heated from one side. A high Prandtl number PCM (lauric acid) was employed. Melting

experiments were performed for different wall temperatures of 55, 60 and 70 °C corresponding to Rayleigh numbers in the range from 3.6×10^8 to 8.3×10^8 and different inclination angles of 0°, 45° and 90°. Qualitative time-dependent flow structures were deduced indirectly from the instantaneous shapes of the solid–liquid interfaces which were confirmed by quantitative temperature results.

Decreasing the inclination angle from the vertical to the horizontal position produces irregular interface shapes and increases the strength of the vortical flow structures in the liquid PCM which tend to three-dimensional chaotic currents for the horizontal enclosure. The shapes of the solid–liquid interfaces during heating in the horizontal enclosure demonstrate the generation of Benard convection cells and development of the cellular structure in the liquid PCM as the melting progresses.

For all inclination angles considered, after the initial period of melting, the melting rate is mainly controlled by induced convection currents in the liquid PCM indicating quasi-steady heat transfer. The rates of melting in the 45° and 90°-inclined enclosures decrease as the height of the solid PCM reduces while the melting rate in the horizontal enclosure remains almost constant until the end of the melting process. It was found that the heat transfer rate of a high Prandtl number PCM being melted from the bottom is almost not affected by the thickness of the liquid layer.

For the range of temperatures considered, the total melting time for the 45° and 0°-inclined enclosures were, on average, 35% and 53% less than the vertical enclosure, respectively. The Nusselt number enhancement ratios, defined as the ratio of time-averaged Nusselt number in the inclined enclosure to that of the vertical enclosure (base case), were found to be 1.7 and 2.1 for the 45° and 0°-inclined enclosures, respectively. These significant enhancement ratios were attributed to the formation of chaotic and multi-cellular flow structures which appeared by decreasing the inclination angle resulting in more heat transfer from the hot wall to the solid–liquid interface. Irrespective of the inclination angle, the time-averaged Nusselt number showed 11% and 35% enhancements when the wall temperature was increased from 55 °C to 60 °C and 70 °C, respectively.

For each inclination angle, the variation of the local heat transfer rates on the solid–liquid interface clearly depicted the regions of the enclosure in which convection currents play the significant role of heat transfer between the liquid PCM and solid interface.

The observed phenomena and measured values can be used to validate numerical simulations relating to the melting process of high Prandtl number PCMs in inclined enclosures.

References

- [1] M.M. Alkilani, K. Sopian, M.A. Alghoul, M. Sofif, M.H. Ruslan, Review of solar air collectors with thermal storage units, *Renewable Sustainable Energy Rev.* 15 (2011) 1476–1490.
- [2] R.M. Muthusivagami, R. Velraj, R. Sethumadhavan, Solar cookers with and without thermal storage – a review, *Renewable Sustainable Energy Rev.* 14 (2010) 691–701.
- [3] T. Arunkumar, D. Denkenberger, A. Ahsan, R. Jayaprakash, The augmentation of distillate yield by using concentrator coupled solar still with phase change material, *Desalination* 314 (2013) 189–192.
- [4] Z. Gu, H. Liu, Y. Li, Thermal energy recovery of air conditioning system – heat recovery system calculation and phase change materials development, *Appl. Therm. Eng.* 24 (2004) 2511–2526.
- [5] U. Strith, V. Butala, Experimental investigation of energy saving in buildings with PCM cold storage, *Int. J. Refrig.* 33 (2010) 1676–1683.
- [6] N.H.S. Tay, M. Belusko, F. Bruno, Designing a PCM storage system using the effectiveness-number of transfer units method in low energy cooling of buildings, *Energy Build.* 50 (2012) 234–242.
- [7] M. Liu, W. Saman, F. Bruno, Development of a novel refrigeration system for refrigerated trucks incorporating phase change material, *Appl. Energy* 92 (2012) 336–342.
- [8] S.C. Fok, W. Shen, F.L. Tan, Cooling of portable hand-held electronic devices using phase change materials in finned heat sinks, *Int. J. Therm. Sci.* 49 (2010) 109–117.

- [9] R. Kandasamy, X. Wang, A.S. Mujumdar, Application of phase change materials in thermal management of electronics, *Appl. Therm. Eng.* 27 (2007) 2822–2832.
- [10] T.Y. Kim, B.S. Hyun, J.J. Lee, J. Rhee, Numerical study of the spacecraft thermal control hardware combining solid–liquid phase change material and a heat pipe, *Aerospace Sci. Technol.* 27 (2012) 10–16.
- [11] T.D. Swanson, G.C. Birur, NASA thermal control technologies for robotic spacecraft, *Appl. Therm. Eng.* 23 (2003) 1055–1065.
- [12] S. Mondal, Phase change materials for smart textiles – an overview, *Appl. Therm. Eng.* 28 (2008) 1536–1550.
- [13] C. Gau, R. Viskanta, Effect of natural convection on solidification from above and melting from below of a pure metal, *Int. J. Heat Mass Transfer* 28 (1985) 573–587.
- [14] C. Gau, R. Viskanta, Melting and solidification of a metal system in a rectangular cavity, *Int. J. Heat Mass Transfer* 27 (1984) 113–123.
- [15] C. Gau, R. Viskanta, Melting and solidification of a pure metal on a vertical wall, *J. Heat Transfer* 108 (1986) 174–181.
- [16] F. Wolff, R. Viskanta, Melting of a pure metal from a vertical wall, *Exp. Heat Transfer* 1 (1987) 17–30.
- [17] C. Beckermann, R. Viskanta, Effect of solid subcooling on natural convection melting of a pure metal, *J. Heat Transfer* 111 (1989) 416–424.
- [18] D.V. Boger, J.W. Westwater, Effect of buoyancy on the melting and freezing process, *J. Heat Transfer* 89 (1967) 81–89.
- [19] N.W. Hale, R. Viskanta, Solid liquid phase change heat transfer and interface motion in materials cooled or heated from above or below, *Int. J. Heat Mass Transfer* 23 (1980) 283–292.
- [20] C. Gau, R. Viskanta, C.J. Ho, Flow visualization during solid–liquid phase change heat transfer II. Melting in a rectangular cavity, *Int. J. Heat Mass Transfer* 10 (1983) 183–190.
- [21] C.J. Ho, R. Viskanta, Heat transfer during melting from an isothermal vertical wall, *J. Heat Transfer* 106 (1984) 12–19.
- [22] B.W. Webb, R. Viskanta, Natural convection dominated melting heat transfer in an inclined rectangular enclosure, *Int. J. Heat Mass Transfer* 29 (1986) 183–192.
- [23] D. Pal, Y.K. Joshi, Melting in a side heated tall enclosure by a uniformly dissipating heat source, *Int. J. Heat Mass Transfer* 44 (2001) 375–387.
- [24] H. Shokouhmand, B. Kamkari, Experimental investigation on melting heat transfer characteristics of lauric acid in a rectangular thermal storage unit, *Exp. Therm. Fluid Sci.* 50 (2013) 201–212.
- [25] E. Assis, L. Katsman, G. Ziskind, R. Letan, Numerical and experimental study of melting in a spherical shell, *Int. J. Heat Mass Transfer* 50 (2007) 1790–1804.
- [26] F.L. Tan, Constrained and unconstrained melting inside a sphere, *Int. Commun. Heat Mass Transfer* 35 (2008) 466–475.
- [27] F.L. Tan, S.F. Hosseini-zadeh, J.M. Khodadadi, L. Fan, Experimental and computational study of constrained melting of phase change materials (PCM) inside a spherical capsule, *Int. J. Heat Mass Transfer* 52 (2009) 3464–3472.
- [28] A. Felix Regin, S.C. Solanki, J.S. Saini, Latent heat thermal energy storage using cylindrical capsule: numerical and experimental investigations, *Renewable Energy* 31 (2006) 2025–2041.
- [29] N.H.S. Tay, F. Bruno, M. Belusko, Comparison of pinned and finned tubes in a phase change thermal energy storage system using CFD, *Appl. Energy* 104 (2013) 79–86.
- [30] R. Baby, C. Balaji, Experimental investigations on phase change material based finned heat sinks for electronic equipment cooling, *Int. J. Heat Mass Transfer* 55 (2012) 1642–1649.
- [31] N. Sharifi, T.L. Bergman, A. Faghri, Enhancement of PCM melting in enclosures with horizontally-finned internal surfaces, *Int. J. Heat Mass Transfer* 54 (2011) 4182–4192.
- [32] K.A.R. Ismail, F.A.M. Lino, Fins and turbulence promoters for heat transfer enhancement in latent heat storage systems, *Exp. Therm. Fluid Sci.* 35 (2011) 1010–1018.
- [33] R. Baby, C. Balaji, Thermal optimization of PCM based pin fin heat sinks: an experimental study, *Appl. Therm. Eng.* 54 (2013) 65–77.
- [34] C.Y. Zhao, W. Lu, Y. Tian, Heat transfer enhancement for thermal energy storage using metal foams embedded within phase change materials (PCMs), *Sol. Energy* 84 (2010) 1402–1412.
- [35] M. Jaworski, Thermal performance of heat spreader for electronics cooling with incorporated phase change material, *Appl. Therm. Eng.* 35 (2012) 212–219.
- [36] C.Y. Zhao, Z.G. Wu, Heat transfer enhancement of high temperature thermal energy storage using metal foams and expanded graphite, *Sol. Energy Mater. Sol. Cells* 95 (2011) 636–643.
- [37] R. Velraj, R. V Seeniraj, B. Hafner, C. Faber, K. Schwarzer, Heat transfer enhancement in a latent heat storage system, *Sol. Energy* 65 (1999) 171–180.
- [38] H.M. Ettooney, I. Alatiqi, M. Al-sahali, S.A. Al-ali, Heat transfer enhancement by metal screens and metal spheres in phase change energy storage systems, *Renewable Energy* 29 (2004) 841–860.
- [39] C.W. Robak, T.L. Bergman, A. Faghri, Enhancement of latent heat energy storage using embedded heat pipes, *Int. J. Heat Mass Transfer* 54 (2011) 3476–3484.
- [40] S. Kalaiselvam, R. Parameshwaran, S. Harikrishnan, Analytical and experimental investigations of nanoparticles embedded phase change materials for cooling application in modern buildings, *Renewable Energy* 39 (2012) 375–387.
- [41] J.M. Khodadadi, S.F. Hosseini-zadeh, Nanoparticle-enhanced phase change materials (NEPCM) with great potential for improved thermal energy storage, *Int. Commun. Heat Mass Transfer* 34 (2007) 534–543.
- [42] S.F. Hosseini-zadeh, A.A.R. Darzi, F.L. Tan, Numerical investigations of unconstrained melting of nano-enhanced phase change material (NEPCM) inside a spherical container, *Int. J. Therm. Sci.* 51 (2012) 77–83.
- [43] F. Frusteri, V. Leonardi, S. Vasta, G. Restuccia, Thermal conductivity measurement of a PCM based storage system containing carbon fibers, *Appl. Therm. Eng.* 25 (2005) 1623–1633.
- [44] J. Fukai, Y. Hamada, Y. Morozumi, O. Miyatake, Improvement of thermal characteristics of latent heat thermal energy storage units using carbon fiber brushes: experiments and modeling, *Int. J. Heat Mass Transfer* 46 (2003) 4513–4525.
- [45] J. Wang, H. Xie, Z. Xin, Y. Li, L. Chen, Enhancing thermal conductivity of palmitic acid based phase change materials with carbon nanotubes as fillers, *Sol. Energy* 84 (2010) 339–344.
- [46] K. Tumuluri, J.L. Alvarado, H. Taherian, C. Marsh, Thermal performance of a novel heat transfer fluid containing multiwalled carbon nanotubes and microencapsulated phase change materials, *Int. J. Heat Mass Transfer* 54 (2011) 5554–5567.
- [47] N.H.S. Tay, F. Bruno, M. Belusko, Experimental investigation of dynamic melting in a tube-in-tank PCM system, *Appl. Energy* 104 (2013) 137–148.
- [48] H. Ozoe, H. Sayama, Natural convection in an inclined rectangular channel at various aspect ratio and angles – experimental measurements, *Int. J. Heat Mass Transfer* 18 (1975) 1425–1431.
- [49] M. Akgu, K. Kaygusuz, Experimental study on melting/solidification characteristics of a paraffin as PCM, *Energy Convers. Manage.* 48 (2007) 669–678.
- [50] N. Sharifi, C.W. Robak, T.L. Bergman, A. Faghri, Three-dimensional PCM melting in a vertical cylindrical enclosure including the effects of tilting, *Int. J. Heat Mass Transfer* 65 (2013) 798–806.
- [51] R. Baby, C. Balaji, Experimental investigations on thermal performance enhancement and effect of orientation on porous matrix filled PCM based heat sink, *Int. Commun. Heat Mass Transfer* 46 (2013) 27–30.
- [52] S.W. Churchill, H.H.S. Chu, Correlating equations for laminar and turbulent free convection from a vertical plate, *Int. J. Heat Mass Transfer* 18 (1975) 1323–1329.
- [53] J.R. Lloyd, W.R. Moran, Natural convection adjacent to horizontal surface of various planforms, *J. Heat Transfer* 96 (1974) 443–447.
- [54] E. Radzemska, W.M. Lewandowski, Heat transfer by natural convection from an isothermal downward-facing round plate in unlimited space, *Appl. Energy* 68 (2001) 347–366.
- [55] L.A. Diaz, R. Viskanta, Visualization of the solid–liquid interface morphology formed by natural convection during melting of a solid from below, *Int. Commun. Heat Mass Transfer* 11 (1984) 35–43.
- [56] B.W. Webb, R. Viskanta, On the characteristic length scale for correlating melting heat transfer data, *Int. Commun. Heat Mass Transfer* 12 (1985) 637–646.
- [57] P. Jany, A. Bejan, Scaling theory of melting with natural convection in an enclosure, *Int. J. Heat Mass Transfer* 31 (1988) 1221–1235.
- [58] C. Beckermann, A general correlation for melting in rectangular enclosure, *J. Heat Transfer* 111 (1989) 1111–1115.
- [59] M. Fteiti, S. Ben Nasrallah, Numerical study of interaction between the fluid structure and the moving interface during the melting from below in a rectangular closed enclosure, *Comput. Mech.* 35 (2004) 161–169.
- [60] S. Kline, F. McClintock, Describing uncertainties in single sample experiments, *Mech. Eng.* 75 (1953) 3–8.